Nonlinear Dyn (2023) 111:9145–9159
https://doi.org/10.1007/s11071-023-08316-x

ORIGINAL PAPER

Asymmetric three-link passive walker

Mahan Jaberi Miandoab · Borhan Beigzadeh

Received: 22 April 2022 / Accepted: 2 February 2023 / Published online: 20 February 2023

Abstract Passive walkers are dynamically stable robots with a gait that resembles the human locomotion. These walkers can be studied to better understand the dynamic behavior of the human gait and design efficient active walkers and assistive devices. In this paper, we study the walking dynamics of a three-link passive walker with an asymmetrical structure where one leg has a knee while the other is knee-less. After finding a 2-periodic steady gait for the three-link walker with humanlike inertial parameters for both legs, the possibility of a gait with symmetrical step lengths is discussed where the half inter-leg angles at the beginning of every step are made equal by altering the physical parameters of the knee-less leg. We further study the gaits with symmetrical step lengths and show that by replacing one leg of a four-link symmetric walker with the knee-less leg of the three-link walker with the symmetrical half inter-leg angles, the dynamic behavior of the kneed leg remains unchanged. This approach can be adapted in the field of gait rehabilitation and prosthesis design to obtain a more symmetrical gait and preserve the motion of the healthy leg.

M. Jaberi Miandoab · B. Beigzadeh (✉)
Biomechatronics and Cognitive Engineering Research Lab, School of Mechanical Engineering, Iran University of Science and Technology, Tehran, Iran
e-mail: b_beigzadeh@iust.ac.ir

M. Jaberi Miandoab
e-mail: moon.mahan@gmail.com

Keywords Passive dynamic walking · Asymmetric walker · Gait rehabilitation · Humanoid bipeds · Chaos

1 Introduction

Passive dynamic walking is a concept that refers to a group of unactuated robots that can maintain a steady gait while walking down a slope. Passive bipedal walkers are dynamically stable, and since their only source of energy is gravity, they have been studied to produce more efficient gaits for actuated robots. Unlike statically stable active walkers like ASIMO [1], passive bipeds display a gait that has likeness to human locomotion. These bipeds, first introduced by McGeer [2, 3], have evolved and become sophisticated through the years. The simplest passive walker [4] is made of two links and acts like an inverted pendulum when one link, called the swing leg, swings forward while the other link, called the stance leg, is in contact with the ground. This two-link model, better known as the compass-like walker [5], has been studied thoroughly over the years to increase accuracy [6], to discuss the basin of attraction of a stable gait [7], and to even obtain a chaotically stable gait [8]. More complex passive walkers are studied by adding ankle stiffness [9] and flat feet to knee-less [10, 11] and kneed models [12]. The addition of knees solves the problem of foot scuffing that exists in compass-like

walkers, while flat feet produce double stance phases in which both feet are in contact with the ground. Another aspect in studying passive walkers is the addition of an upper body. The upper body can be kept upright passively by using springs [13] or kinematic couplings [14]. Moreover, steady gaits for three-dimensional passive walkers have been found by gradually transforming a planar walker into a 3D walker [15]. Two-dimensional [16] and three-dimensional [17, 18] walkers have been built based on the concept of passive dynamic walking to better study the effects of exerting changes in the structure of the biped. Recent studies have also extended the concept of three-dimensional passive walking to passive turning and curved walking [19, 20]. The concept of passive dynamic walking is mostly used to design efficient locomotion in actively and passivity-based controlled robots [21]. Different aspects of a passive walker can be improved by using various control methods. In a study by Kobayashi et al. [22], an adaptive speed controller is proposed for a three-dimensional walker to control the speed of forward and sideward movement. In two studies by Gritli et al. [23, 24], the chaotic behavior of a torso-driven semi-passive walker is controlled by using an OGY-based controller, while another study [25] focuses on stabilization of a compass-like walker by developing the analytical expression of the controlled Poincaré map. Simple and light manipulators are preferred in industrial applications [26]. Therefore, passive walkers have also been studied to design passive object manipulators for efficient manipulation without actuators [27, 28]. Since passive walkers resemble the human gait in terms of being dynamically stable, they can be used to design prostheses [29], exoskeletons [30], and rehabilitation methods [31] and better understand the asymmetrical gait in people with nervous system damage such as stroke patients [32]. These studies focus on kneed walkers, and the asymmetrical behavior arises from changing the inertial parameters and the location of knee in one leg. Another recent study focuses on an asymmetric underactuated walker where one leg has a knee while the other leg is knee-less [33]. The asymmetrical behavior of this walker stems from the structural differences of the legs and will exist even for symmetrical inertial parameters for legs. Inspired by the underactuated walker discussed in [33], the aim of the present research is to find a steady gait for an asymmetric three-link passive walker with humanlike inertial parameters. Moreover, the possibility of a more symmetrical motion is studied by changing the physical parameters of the knee-less leg to obtain a gait with symmetrical step lengths. Gait asymmetry in terms of varying step lengths is present in stroke patients [34] and lower-limb amputees [35]. While the simulations are performed for an extreme case of asymmetry, the approach taken in this study to obtain the desired gait can be followed and adapted in the field of robotics and designing orthoses and prostheses for gait rehabilitation where other cases of physical asymmetry are present.

2 Dynamic modeling

The planar asymmetric three-link walker presented here has point feet and is assumed to be pinned to the ground at the stance foot for each step. One leg has a passive knee made of two links called the thigh and the shank, while the other leg is knee-less and is modeled as a single link. To make the results comparable to human walking for gait rehabilitation and other applications, the walker has anthropomorphic parameters, meaning that the length and inertial parameters of the legs are similar to that of a human. These parameters are extracted from [36] for a 60 kg female, which are given in Table 1.

The presented model walks on a slope with the angle γ as depicted in Fig. 1 where m_s, m_t, m_p and m_h are the mass center of the shank, mass center of the thigh, mass center of the knee-less leg and the point mass of the hip, respectively. The three angles q_s, q_t and q_p are the absolute angles of the shank, the thigh and the knee-less leg, respectively.

Owing to the asymmetrical characteristics of this model, consecutive steps will differ in terms of their dynamic behavior. As such, assuming that the first step is taken by the kneed leg, odd and even steps are modeled as follows.

In odd steps, the knee-less leg is pinned to the ground as the kneed leg swings forward. These steps consist of two phases where the swing knee is unlocked at first until the kneed leg extends and the knee strike occurs. We assume that there is a locking mechanism in the knee which remains locked after the impact and keeps the absolute angles of the shank and

Table 1 Values for the parameters of the three-link asymmetric walker with symmetrical inertial parameters

Symbol	Description	Value
a_1	Shank length between mass center and foot	0.231 m
b_1	Shank length between mass center and knee	0.157 m
a_2	Thigh length between mass center and knee	0.236 m
b_2	Thigh length between mass center and Hip	0.143 m
a_p	Knee-less leg length between mass center and foot	0.532 m
b_p	Knee-less leg length between mass center and hip	0.235 m
m_h	Hip mass	37.08 kg
m_t	Thigh mass	8.76 kg
m_s	Shank mass	2.70 kg
m_p	Knee-less leg mass	11.46 kg
J_t	Mass moment of inertia of thigh	0.129 kg.m^2
J_s	Mass moment of inertia of shank	0.032 kg.m^2
J_p	Mass moment of inertia of the knee-less leg	0.479 kg.m^2

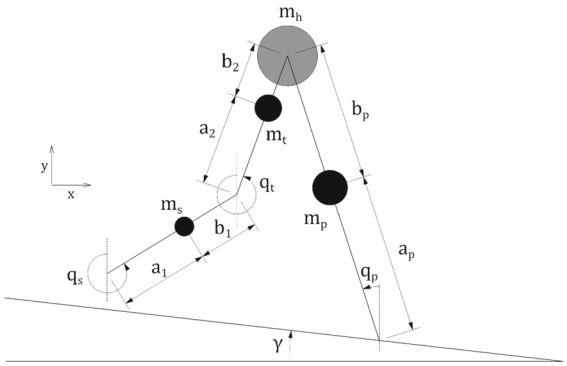

Fig. 1 Three-link asymmetric passive walker model

the thigh equal during the rest of the step. The step ends with the impact of the swing foot with the ground, and the roles of the legs are switched to start the next step.

In even steps, the kneed leg is in contact with the ground and the knee remains locked for the duration of the step. These steps are similar to two-link compass gait models as the knee-less leg swings forward until the swing foot touches the ground. We ignore the foot scuffing that occurs in this phase. The roles of legs are switched, and the knee of the new swing leg is unlocked to start the next step. The phases explained are shown in Fig. 2.

2.1 Walking dynamics

2.1.1 Continuous phase

The walker's configuration for odd steps can be defined by the generalized coordinates $q_{\mathrm{OU}} = \left[q_{\mathrm{pst}}, q_{\mathrm{tsw}}, q_{\mathrm{ssw}}\right]$ for the unlocked-knee phase and $q_{\mathrm{OL}} = \left[q_{\mathrm{pst}}, q_{\mathrm{sw}}\right]$ for the locked-knee phase of the step. The subscripts st and sw specify the role of the legs as the stance leg and the swing leg, respectively. The subscript p stands for the parameters of the knee-less leg, while the subscripts t and s stand for the parameters of the thigh and the shank of the kneed leg. Apart from the legs having different roles, the generalized coordinates for even steps are similar to the second phase of odd steps. The state vectors for odd and even steps are then as follows:

$$x_{\mathrm{OU}} = \left[q_{\mathrm{pst}}, q_{\mathrm{tsw}}, q_{\mathrm{ssw}}, \dot{q}_{\mathrm{pst}}, \dot{q}_{\mathrm{tsw}}, \dot{q}_{\mathrm{ssw}}\right], \tag{1}$$

$$x_{\mathrm{OL}} = \left[q_{pst}, q_{\mathrm{sw}}, \dot{q}_{\mathrm{pst}}, \dot{q}_{\mathrm{sw}}\right], \tag{2}$$

$$x_E = \left[q_{\mathrm{st}}, q_{\mathrm{psw}}, \dot{q}_{\mathrm{st}}, \dot{q}_{\mathrm{psw}}\right] \tag{3}$$

The dynamic equations of motion for these continuous phases are derived by using the following equation:

$$M(q)\ddot{q} + N(q,\dot{q})\dot{q} + G(q) = 0, \tag{4}$$

where M is the inertia matrix, N is the Coriolis matrix and G is the gravity vector. Equation (4) can be written in the state-space form as follows:

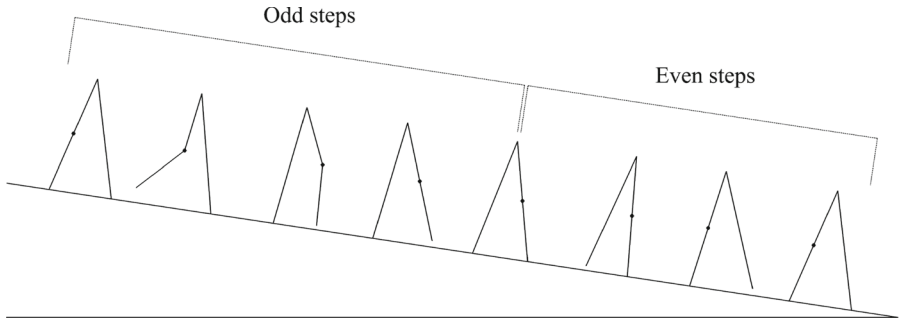

Fig. 2 Walking phases of the asymmetric walker for two steps

$$\dot{x} = \begin{bmatrix} \dot{q} \\ \ddot{q} \end{bmatrix} = \begin{bmatrix} \dot{q} \\ -M(q)^{-1}[N(q,\dot{q})\dot{q} + G(q)] \end{bmatrix} \tag{5}$$

2.1.2 Transition equations

There are three impacts that occur during every two steps. We assume that these impacts are fully inelastic and instantaneous and find the angular velocity of each link by using the transitional equations derived from the conservation of angular momentum theorem.

2.1.2.1 Knee strike The knee strike happens during odd steps when the kneed leg swings forward until it is fully extended. Three equations are needed to calculate the angular velocities of the links after impact. Two equations are derived by noting that the angular momentum of the whole walker is conserved about the stance foot and the angular momentum of the swing leg is conserved about the hip. These angular momentums are calculated as explained in [37] by using the following equations:

$$\begin{aligned} \boldsymbol{L}_{F1}^{-} = {} & m_p\left(\boldsymbol{F}_1\boldsymbol{P}_{\mathrm{st}} \wedge \boldsymbol{v}_{\mathrm{pst}}^{-}\right) + J_p\dot{q}_{\mathrm{pst}}^{-} + m_H\left(\boldsymbol{F}_1\boldsymbol{H} \wedge \boldsymbol{v}_{H}^{-}\right) \\ & + m_t\left(\boldsymbol{F}_1\boldsymbol{T}_{\mathrm{sw}} \wedge \boldsymbol{v}_{\mathrm{tsw}}^{-}\right) + J_t\dot{q}_{\mathrm{tsw}}^{-} \\ & + m_s\left(\boldsymbol{F}_1\boldsymbol{S}_{\mathrm{sw}} \wedge \boldsymbol{v}_{\mathrm{ssw}}^{-}\right) + J_s\dot{q}_{\mathrm{ssw}}^{-}, \end{aligned} \tag{6}$$

$$\begin{aligned} \boldsymbol{L}_{F1}^{+} = {} & m_p\left(\boldsymbol{F}_1\boldsymbol{P}_{\mathrm{st}} \wedge \boldsymbol{v}_{\mathrm{pst}}^{+}\right) + J_p\dot{q}_{\mathrm{pst}}^{+} + m_H\left(\boldsymbol{F}_1\boldsymbol{H} \wedge \boldsymbol{v}_{H}^{+}\right) \\ & + m_t\left(\boldsymbol{F}_1\boldsymbol{T}_{\mathrm{sw}} \wedge \boldsymbol{v}_{\mathrm{tsw}}^{+}\right) + J_t\dot{q}_{\mathrm{tsw}}^{+} \\ & + m_s\left(\boldsymbol{F}_1\boldsymbol{S}_{\mathrm{sw}} \wedge \boldsymbol{v}_{\mathrm{ssw}}^{+}\right) + J_s\dot{q}_{\mathrm{ssw}}^{+}, \end{aligned} \tag{7}$$

$$\begin{aligned} \boldsymbol{L}_{H}^{-} = {} & m_t\left(\boldsymbol{H}\boldsymbol{T}_{\mathrm{sw}} \wedge \boldsymbol{v}_{\mathrm{tsw}}^{-}\right) + J_t\dot{q}_{\mathrm{tsw}}^{-} + m_s\left(\boldsymbol{H}\boldsymbol{S}_{\mathrm{sw}} \wedge \boldsymbol{v}_{\mathrm{ssw}}^{-}\right) \\ & + J_s\dot{q}_{\mathrm{ssw}}^{-}, \end{aligned} \tag{8}$$

$$\begin{aligned} \boldsymbol{L}_{H}^{+} = {} & m_t\left(\boldsymbol{H}\boldsymbol{T}_{\mathrm{sw}} \wedge \boldsymbol{v}_{\mathrm{tsw}}^{+}\right) + J_t\dot{q}_{\mathrm{tsw}}^{+} + m_s\left(\boldsymbol{H}\boldsymbol{S}_{\mathrm{sw}} \wedge \boldsymbol{v}_{\mathrm{ssw}}^{+}\right) \\ & + J_s\dot{q}_{\mathrm{ssw}}^{+}, \end{aligned} \tag{9}$$

where L_{F1} is the angular momentum of the walker about the stance foot, L_H is the angular momentum of the swing leg about the hip and v is the absolute velocity of the mass center specified by the subscript. The points P, T, S,H and F_1 indicate the mass center of the knee-less leg, mass center of the thigh, mass center of the shank, the hip and the position of the trailing foot, respectively. The superscripts $+$ and $-$ denote the post-impact and the pre-impact parameters, and the subscripts s, t, p, sw and st specify the parameters related to the shank of the kneed leg, thigh of the kneed leg, the knee-less leg, the swing leg and the stance leg, respectively. The inertial parameters are defined as given in Table 1. The wedge product of two vectors $a = [a_1; a_2]$ and $b = [b_1; b_2]$ is defined as:

$$a \wedge b = a_1 b_2 - a_2 b_1 \tag{10}$$

The third equation is obtained from the assumption that the kneed leg remains extended and the knee is locked after impact. The three transition equations for the knee strike are then:

$$\boldsymbol{L}_{F1}^{-} = \boldsymbol{L}_{F1}^{+}, \tag{11}$$

$$\boldsymbol{L}_{H}^{-} = \boldsymbol{L}_{H}^{+}, \tag{12}$$

$$\dot{q}_{\mathrm{tsw}}^{+} = \dot{q}_{\mathrm{ssw}}^{+} \tag{13}$$

2.1.2.2 Heel strike in odd steps We assume that there are no double stance phases and the legs switch roles instantaneously after impact. This means that the angular momentum of the walker is conserved about the swing foot and the angular momentum of the stance leg is conserved about the hip, which are calculated before and after the impact as follows:

$$\begin{aligned}\boldsymbol{L}_{F2}^{-} = {} & m_s\left(\boldsymbol{F}_2\boldsymbol{S}_{\mathrm{sw}} \wedge \boldsymbol{v}_{\mathrm{ssw}}^{-}\right) + J_s\dot{q}_{\mathrm{sw}}^{-} + m_t\left(\boldsymbol{F}_2\boldsymbol{T}_{\mathrm{sw}} \wedge \boldsymbol{v}_{\mathrm{tsw}}^{-}\right) \\ & + J_t\dot{q}_{\mathrm{sw}}^{-} + m_H\left(\boldsymbol{F}_2\boldsymbol{H} \wedge \boldsymbol{v}_{H}^{-}\right) + m_p\left(\boldsymbol{F}_2\boldsymbol{P}_{\mathrm{st}} \wedge \boldsymbol{v}_{\mathrm{pst}}^{-}\right) \\ & + J_p\dot{q}_{\mathrm{pst}}^{-},\end{aligned} \tag{14}$$

$$\begin{aligned}\boldsymbol{L}_{F2}^{+} = {} & m_s\left(\boldsymbol{F}_2\boldsymbol{S}_{\mathrm{st}} \wedge \boldsymbol{v}_{\mathrm{sst}}^{+}\right) + J_s\dot{q}_{\mathrm{st}}^{+} + m_t\left(\boldsymbol{F}_2\boldsymbol{T}_{\mathrm{st}} \wedge \boldsymbol{v}_{\mathrm{tst}}^{+}\right) \\ & + J_t\dot{q}_{\mathrm{st}}^{+} + m_H\left(\boldsymbol{F}_2\boldsymbol{H} \wedge \boldsymbol{v}_{H}^{+}\right) \\ & + m_p\left(\boldsymbol{F}_2\boldsymbol{P}_{\mathrm{sw}} \wedge \boldsymbol{v}_{\mathrm{psw}}^{+}\right) + J_p\dot{q}_{\mathrm{psw}}^{+},\end{aligned} \tag{15}$$

$$\boldsymbol{L}_{H}^{-} = m_p\left(\boldsymbol{H}\boldsymbol{P}_{\mathrm{st}} \wedge \boldsymbol{v}_{\mathrm{pst}}^{-}\right) + J_p\dot{q}_{\mathrm{pst}}^{-}, \tag{16}$$

$$\boldsymbol{L}_{H}^{+} = m_p\left(\boldsymbol{H}\boldsymbol{P}_{\mathrm{sw}} \wedge \boldsymbol{v}_{\mathrm{psw}}^{+}\right) + J_p\dot{q}_{\mathrm{psw}}^{+}, \tag{17}$$

where F_2 indicates the position of the leading foot.

The kneed leg, which becomes the new stance leg after impact, remains extended during even steps, so the angular velocity of the thigh and the shank of this leg remain equal after impact. The equations needed to obtain the post-impact angular velocity of the legs are then:

$$\boldsymbol{L}_{F2}^{-} = \boldsymbol{L}_{F2}^{+}, \tag{18}$$

$$\boldsymbol{L}_{H}^{-} = \boldsymbol{L}_{H}^{+}, \tag{19}$$

$$\dot{q}_{\mathrm{sst}}^{+} = \dot{q}_{\mathrm{tst}}^{+} = \dot{q}_{\mathrm{st}}^{+} \tag{20}$$

2.1.2.3 Heel strike in even steps By assuming that locking mechanism in the kneed leg is unlocked after this impact occurs, we can conclude that the thigh and the shank of this leg, which becomes the new swing leg, have equal angular velocities after impact. The remaining equations needed are derived from the angular momentum of the walker being conserved about the swing foot and the angular momentum of the stance leg being conserved about the hip as follows:

$$\begin{aligned}\boldsymbol{L}_{F2}^{-} = {} & m_p\left(\boldsymbol{F}_2\boldsymbol{P}_{\mathrm{sw}} \wedge \boldsymbol{v}_{\mathrm{psw}}^{-}\right) + J_p\dot{q}_{\mathrm{psw}}^{-} + m_H\left(\boldsymbol{F}_2\boldsymbol{H} \wedge \boldsymbol{v}_{H}^{-}\right) \\ & + m_t\left(\boldsymbol{F}_2\boldsymbol{T}_{\mathrm{st}} \wedge \boldsymbol{v}_{\mathrm{tst}}^{-}\right) + J_t\dot{q}_{\mathrm{st}}^{-} + m_s\left(\boldsymbol{F}_2\boldsymbol{S}_{\mathrm{st}} \wedge \boldsymbol{v}_{\mathrm{sst}}^{-}\right) \\ & + J_s\dot{q}_{\mathrm{st}}^{-},\end{aligned} \tag{21}$$

$$\begin{aligned}\boldsymbol{L}_{F2}^{+} = {} & m_p\left(\boldsymbol{F}_2\boldsymbol{P}_{\mathrm{st}} \wedge \boldsymbol{v}_{\mathrm{pst}}^{+}\right) + J_p\dot{q}_{\mathrm{pst}}^{+} + m_H\left(\boldsymbol{F}_2\boldsymbol{H} \wedge \boldsymbol{v}_{H}^{+}\right) \\ & + m_t\left(\boldsymbol{F}_2\boldsymbol{T}_{\mathrm{sw}} \wedge \boldsymbol{v}_{\mathrm{tsw}}^{+}\right) + J_t\dot{q}_{\mathrm{tsw}}^{+} \\ & + m_s\left(\boldsymbol{F}_2\boldsymbol{S}_{\mathrm{sw}} \wedge \boldsymbol{v}_{\mathrm{ssw}}^{+}\right) + J_s\dot{q}_{\mathrm{ssw}}^{+},\end{aligned} \tag{22}$$

$$\begin{aligned}\boldsymbol{L}_{H}^{-} = {} & m_t\left(\boldsymbol{H}\boldsymbol{T}_{\mathrm{st}} \wedge \boldsymbol{v}_{\mathrm{tst}}^{-}\right) + J_t\dot{q}_{\mathrm{st}}^{-} + m_s\left(\boldsymbol{H}\boldsymbol{S}_{\mathrm{st}} \wedge \boldsymbol{v}_{\mathrm{sst}}^{-}\right) \\ & + J_s\dot{q}_{\mathrm{st}}^{-},\end{aligned} \tag{23}$$

$$\begin{aligned}\boldsymbol{L}_{H}^{+} = {} & m_t\left(\boldsymbol{H}\boldsymbol{T}_{\mathrm{sw}} \wedge \boldsymbol{v}_{\mathrm{tsw}}^{+}\right) + J_t\dot{q}_{\mathrm{tsw}}^{+} + m_s\left(\boldsymbol{H}\boldsymbol{S}_{\mathrm{sw}} \wedge \boldsymbol{v}_{\mathrm{ssw}}^{+}\right) \\ & + J_s\dot{q}_{\mathrm{ssw}}^{+},\end{aligned} \tag{24}$$

$$\boldsymbol{L}_{F_2}^{-} = \boldsymbol{L}_{F_2}^{+}, \tag{25}$$

$$\boldsymbol{L}_{H}^{-} = \boldsymbol{L}_{H}^{+}, \tag{26}$$

$$\dot{q}_{\mathrm{tsw}}^{+} = \dot{q}_{\mathrm{ssw}}^{+} \tag{27}$$

The transitional equations are solved when impact is detected during the continuous phases to obtain the velocities of the links post-impact to be used to simulate the next continuous phase.

2.2 Numerical simulation and stability

Because of the asymmetrical nature of the walker, we try to find a 2-periodic stable gait. To do so, we define a Poincaré map for every two steps and choose the start of each step, right after a heel strike, as our Poincaré section. The 2-periodic gait is stable if the fixed point found for this Poincaré map corresponds to a limit cycle that attracts nearby trajectories. The Poincaré map described can be formulated as follows:

$$x_{k+2} = F(x_k), \tag{28}$$

where x_k is the state vector of the kth step at the beginning of each step. A fixed point x^* for this map is defined as follows:

$$x^* = F(x^*) \tag{29}$$

Fixed points can be found by minimizing the function $G(x)$:

$$G(x) = F(x) - x \tag{30}$$

To study the stability of the fixed point, we can linearize Eq. (29) for small perturbations δx as follows:

$$F(x^* + \delta x) \approx F(x^*) + J\delta x \tag{31}$$

where the Jacobian J is obtained by making small perturbations in state variables as explained in [5]. For x^* to be a stable fixed point of the mapping F, for small perturbations, the state vector of the following steps should be closer to the fixed point. This means that the eigenvalues of J should have absolute values less than one. The nonlinear dynamic equations are solved numerically by using the ODE45 algorithm in MATLAB, and the instant changes in the angular velocity of the links at impacts are calculated by using the transitional equations.

3 Results and discussion

We started our search for a stable gait with similar inertial parameters for both legs. By minimizing the function $G(x)$ over two steps with the global search optimization function in MATLAB, a 2-periodic gait was quickly found on the slope angle of 0.04 rad. Figures 3, 4 and 5 are the limit cycles for the shank, thigh and knee-less leg over two steps, respectively. In these figures, the letter A indicates the start of odd steps, in which the kneed leg takes on the role of the swing leg while the knee-less leg is the stance leg. The shank of the kneed leg swings forward until the knee strike occurs at B and the angular velocity of the legs is changed instantaneously to the values at C. The kneed leg, which remains extended after the knee strike, has an impact with the ground at D where the roles of the legs are changed and the knee-less leg becomes the new swing leg in an instant. The knee of the kneed leg remains locked through E to A and is unlocked after the impact of knee-less leg with the ground at F.

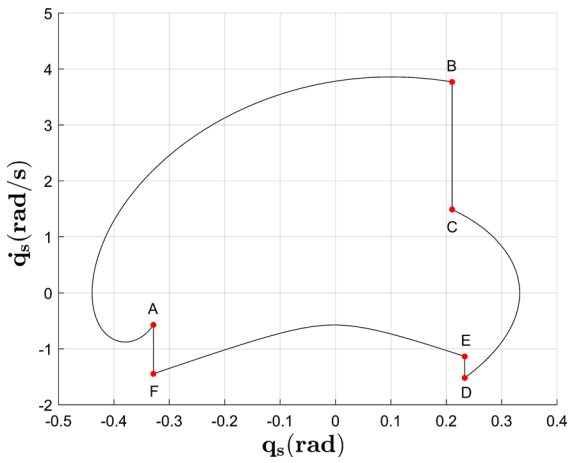

Fig. 3 Limit cycle of the shank of the kneed leg over two consecutive steps on the slope angle of 0.04 rad. The points A–F denote the impacts that occur throughout the gait

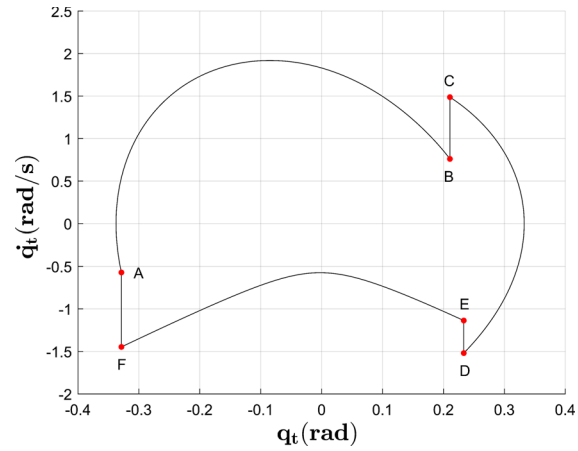

Fig. 4 Limit cycle of the thigh of the kneed leg over two consecutive steps on the slope angle of 0.04 rad. The points A–F denote the impacts that occur throughout the gait

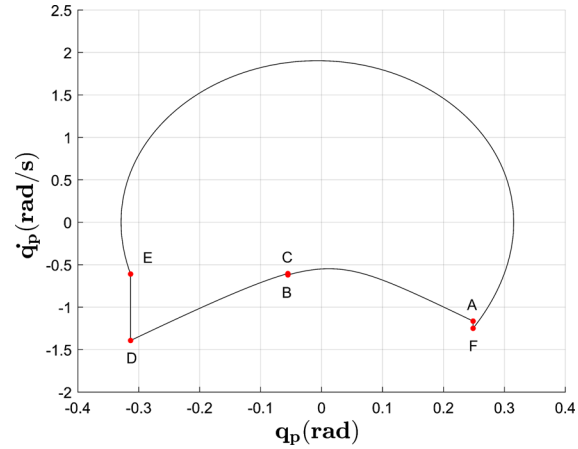

Fig. 5 Limit cycle of the knee-less leg over two consecutive steps on the slope angle of 0.04 rad. The points A–F denote the impacts that occur throughout the gait

Other 2-periodic stable gaits can be found for slope angles between 0.0235 rad and 0.0470 rad. By further increasing the slope angle, period doublings occur which result in 4-periodic and 8-periodic gaits. This trend continues until no periodicity can be detected and the gait becomes chaotic. These period doublings can be shown in bifurcation diagrams of the half inter-leg angle at the beginning of steps with respect to the slope angle as depicted in Fig. 6.

We can alter the dynamic behavior of this model without changing the leg parameters by introducing damping in knee. Small amounts of damping can alter the stability of the system and increase the slope angle range in which a stable gait can be found. The bifurcation diagram for the half inter-leg angle at the beginning of steps with respect to the slope angle is plotted for the damping coefficients of $c = 0.1\,\frac{\text{Nms}}{\text{rad}}$ in Fig. 7.

It is clear that the damping in the knee should be regarded as a determining factor in the resulting gaits for the walker. For example, in the case of the damping coefficient equal to $0.1\,\frac{\text{Nms}}{\text{rad}}$ (Fig. 7), 2-periodic steady gaits are possible in slope angles of 0.0172 rad to 0.0505 rad which is a wider range compared to the model with no damping in the knee (Fig. 6).

3.1 Asymmetric gaits with symmetrical half inter-leg angles

While a 1-periodic gait cannot be expected from a structurally asymmetric walker, a symmetrical gait is generally preferred for walking robots. This

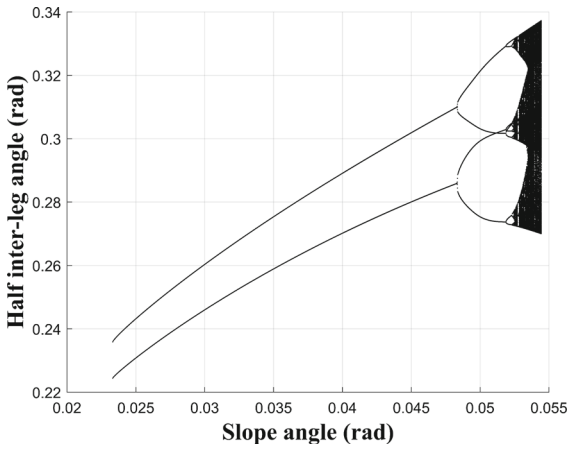

Fig. 6 Bifurcation diagram of the half inter-leg angle at the beginning of steps with respect to the slope angle

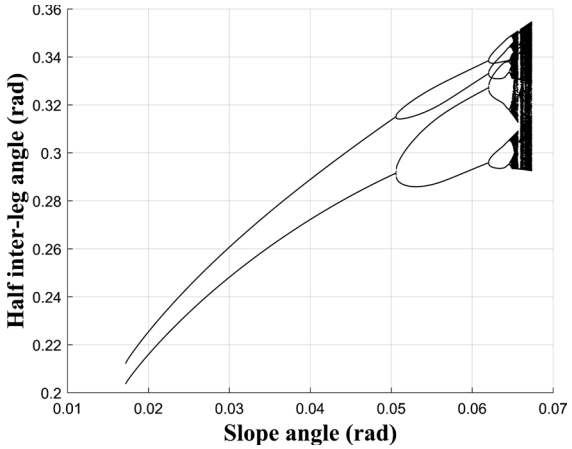

Fig. 7 Bifurcation diagram of the half inter-leg angle at the beginning of steps with respect to the slope angle for $c = 0.1\,\frac{\text{Nms}}{\text{rad}}$

symmetrical behavior can be obtained in the form of symmetrical step lengths. The legs in the three-link model are structurally different and will exhibit different swinging motions unless the knee of the kneed leg is completely locked or a knee is added to the knee-less leg. Regardless of the natural asymmetrical dynamics of this walker, the half inter-leg angle at the beginning of each step can be equal which will result in symmetrical step lengths. The thigh and the shank of the kneed leg have the same absolute angles at the beginning of odd and even steps. As a result, if α, the half inter-leg angle, is equal at the start of these steps, the odd and even steps of the resulting gait will consist of equal step lengths. α for odd and even steps is defined as shown in Fig. 8.

It is apparent from the bifurcation diagrams that the two branches of α do not intersect in 2-periodic gaits over different slopes. To study the possibility of symmetrical half inter-leg angles, we assume that the inertial parameters of the knee-less leg are configurable. By doing this, we can obtain the bifurcation diagram of α with respect to the mass of the knee-less leg for different values of the damping in the knee of the kneed leg, the mass center position of the knee-less leg and the mass moment of inertia of this leg at the slope angle of 0.04 rad to see if there are any intersections between the branches of 2-periodic stable gaits. First, we discuss the effect of the damping coefficient on the bifurcation diagram of α with respect to the mass of the knee-less leg by keeping the remaining inertial parameters of the knee-less leg similar to the kneed leg. Based on Fig. 9, we observe

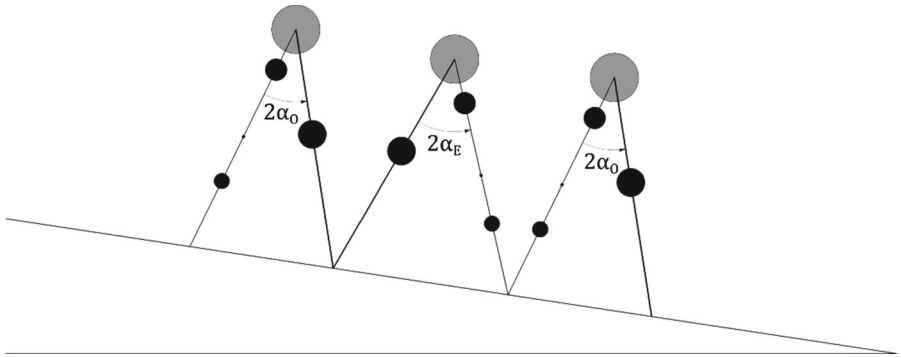

Fig. 8 Half inter-leg angles α_O and α_E for odd and even steps, respectively

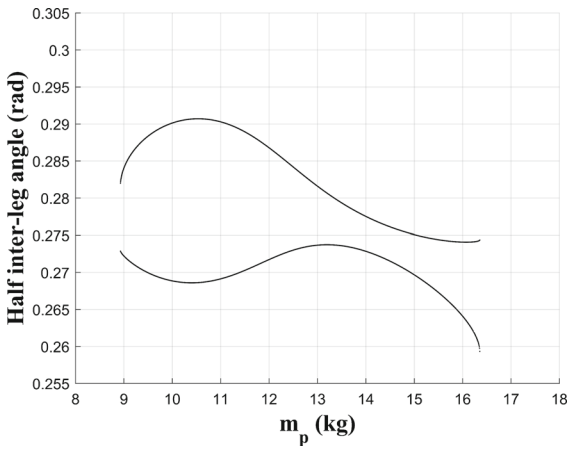

Fig. 9 Bifurcation diagram of the half inter-leg angle at the beginning of steps with respect to the mass of the knee-less leg for the model with no damping in the knee of the kneed leg

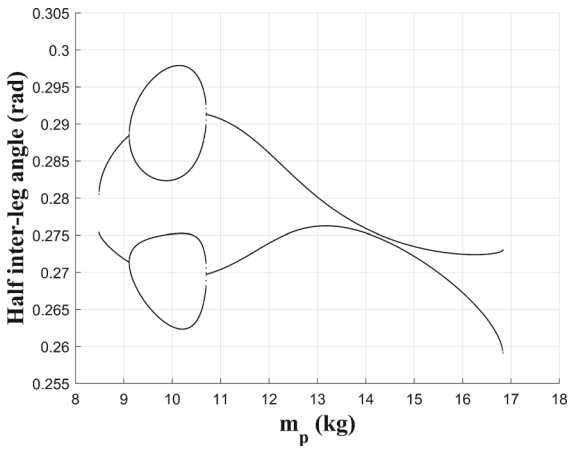

Fig. 10 Bifurcation diagram of the half inter-leg angle at the beginning of steps with respect to the mass of the knee-less leg for $c = 0.08\,\frac{\text{Nms}}{\text{rad}}$

that when no damping is present in the knee, the two branches of the 2-periodic gaits do not cross and gaits with symmetrical half inter-leg angles are not possible. This is changed by increasing the damping coefficient in the knee of the kneed leg as it is observed in Fig. 10, that for the damping coefficient of $0.08\,\frac{\text{Nms}}{\text{rad}}$, the two branches become significantly closer in addition to 4-periodic gaits being formed in lower masses. By further increasing the damping in the knee, gaits with the desired pattern are obtainable for specific masses of the knee-less leg. This is depicted in Fig. 11 for the damping coefficient of $0.18\,\frac{\text{Nms}}{\text{rad}}$.

The two values for m_p that result in symmetric half inter-leg angles are further away for higher values of the damping coefficient. These values are 13.06 kg and 15.68 kg for the damping coefficient of $0.18\,\frac{\text{Nms}}{\text{rad}}$. These mass values are significantly higher than the mass of

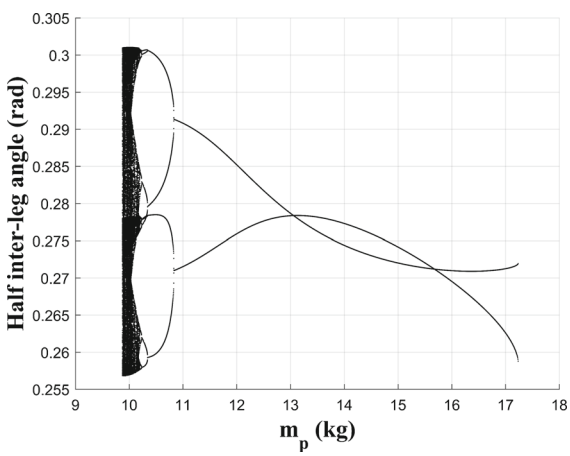

Fig. 11 Bifurcation diagram of the half inter-leg angle at the beginning of steps with respect to the mass of the knee-less leg for $c = 0.18\,\frac{\text{Nms}}{\text{rad}}$

the kneed leg. It is desirable for walking robots to have symmetric leg masses. In addition, in clinical applications, the masses of prosthetic legs are often designed to be lower than that of a human leg. As a result, we alter the location of the mass center and value of the mass moment of inertia of the knee-less leg to study the possibility of obtaining a more symmetrical gait for a model where the mass of the knee-less leg is equal to or lower than the mass of the kneed leg. To ensure the crossing of the two branches in the bifurcation diagrams, the damping coefficient of the knee is kept at $0.18\,\frac{\text{Nms}}{\text{rad}}$.

The value for center of mass of the knee-less leg is described as the distance between the foot and the center of mass. By increasing the center of mass from 0.532 to 0.6 m, it is observed in Fig. 12 that the intersections occur at higher mass values, which is not preferred. With a lower center of mass value of 0.4 m, however, the branches no longer collide in the 2-periodic region as shown in Fig. 13. An increase in the damping coefficient from 0.15 $\frac{\text{Nms}}{\text{rad}}$ to 0.35 $\frac{\text{Nms}}{\text{rad}}$ in Fig. 14 will make 2-periodic gaits with symmetrical half inter-leg angles possible, but the mass for the symmetrical α is still above the mass of the kneed leg.

The next step is to change the value of the mass moment of inertia of the knee-less leg, while the center of mass is kept similar to the other leg. We observe in Fig. 15 that by lowering the mass moment of inertia to 0.400 kg.m^2 from 0.479 kg.m^2, the gaits with symmetrical half inter-leg angles are obtainable at lower knee-less leg masses, which is the desired

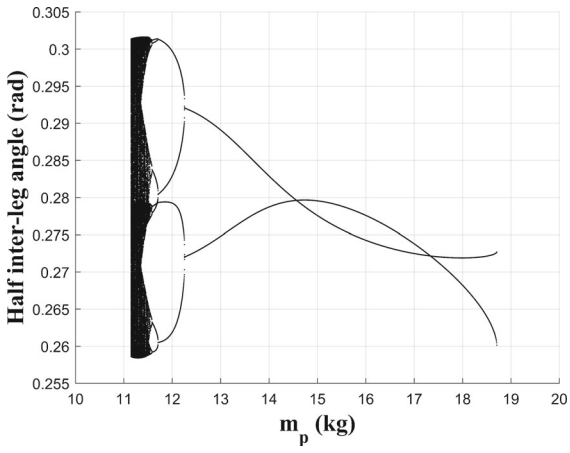

Fig. 12 Bifurcation diagram of the half inter-leg angle at the beginning of steps with respect to the mass of the knee-less leg for $c = 0.18\,\frac{\text{Nms}}{\text{rad}}$ and COM of 0.6 m

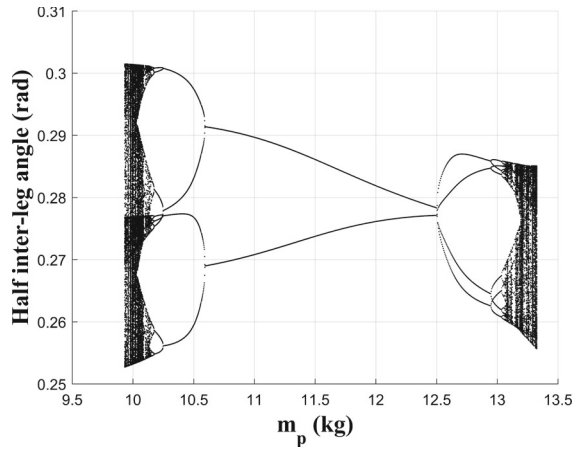

Fig. 13 Bifurcation diagram of the half inter-leg angle at the beginning of steps with respect to the mass of the knee-less leg for $c = 0.18\,\frac{\text{Nms}}{\text{rad}}$ and COM of 0.4 m

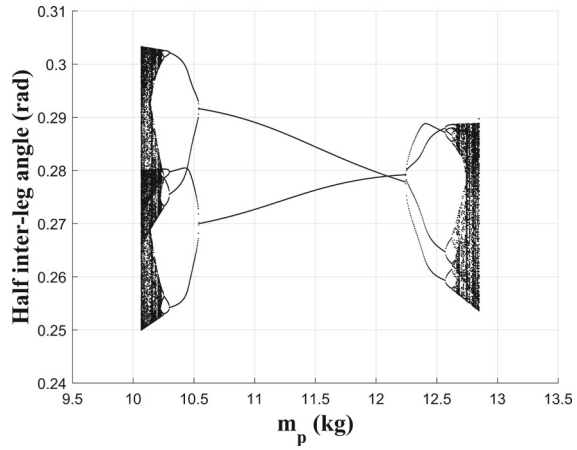

Fig. 14 Bifurcation diagram of the half inter-leg angle at the beginning of steps with respect to the mass of the knee-less leg for $c = 0.35\,\frac{\text{Nms}}{\text{rad}}$ and COM of 0.4 m

outcome. Lower moments of inertia mean that the mass of the leg is concentrated closer to the mass center.

We can use these findings to simulate a gait with symmetric values for α by just lowering the mass moment of inertia while the mass and the center of mass of the knee-less leg are kept similar to the kneed leg. In this case, the required mass moment of inertia for the knee-less leg is 0.375 kg.m^2. A side-by-side comparison of the limit cycles between the walker with symmetrical inertial parameters (Fig. 16a) and the walker with the symmetrical α (Fig. 16b) is provided in Fig. 16. Both of these gaits are for the

knee damping coefficient of 0.18 $\frac{\text{Nms}}{\text{rad}}$ on the slope angle of 0.04 rad. In the case of the walker with the more symmetrical gait (Fig. 16b), it is apparent that the absolute angles of the stance and swing legs at the beginning of odd steps are equal to those of even steps and the dynamic behavior of the stance legs is nearly identical.

Similarly, by further decreasing the mass moment of inertia of the knee-less leg, more symmetrical stable gaits can be simulated for cases where the mass of the knee-less leg is lower than the kneed leg. This is demonstrated in Fig. 17 where the mass moment of inertia of the knee-less leg is set to 0.1128 and the gaits with symmetrical half inter-leg angles are obtainable for knee-less leg masses of 6 kg and 8 kg.

3.2 A two-mass system with variable mass moment of inertia

Based on our findings in the previous section, we conclude that by changing the mass moment of inertia of the knee-less leg, we can obtain a gait that is symmetrical in terms of the half inter-leg angle at the beginning of steps. It is important to note that to achieve this on different slope angles, different values for the mass moment of inertia are needed. To address

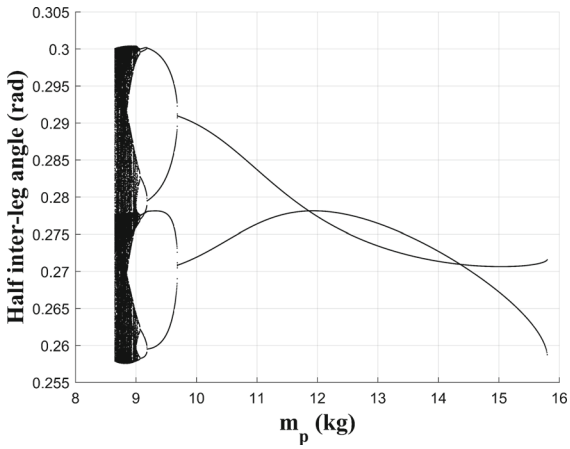

Fig. 15 Bifurcation diagram of the half inter-leg angle at the beginning of steps with respect to the mass of the knee-less leg for $c = 0.18\frac{\text{Nms}}{\text{rad}}$ and MOI of $0.4kg.m^2$

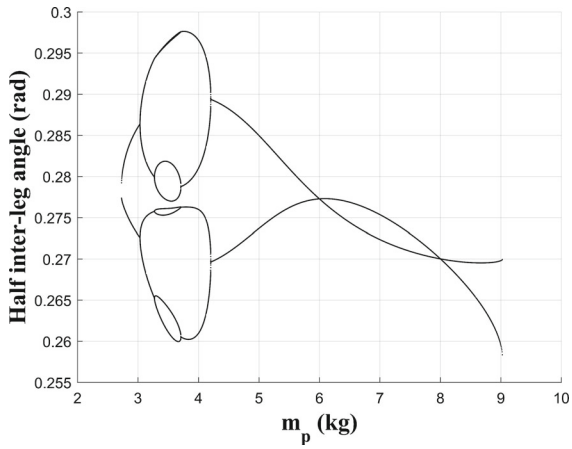

Fig. 17 Bifurcation diagram of the half inter-leg angle at the beginning of steps with respect to the mass of the knee-less leg for $c = 0.18\frac{\text{Nms}}{\text{rad}}$ and MOI of 0.1128kg.m^2

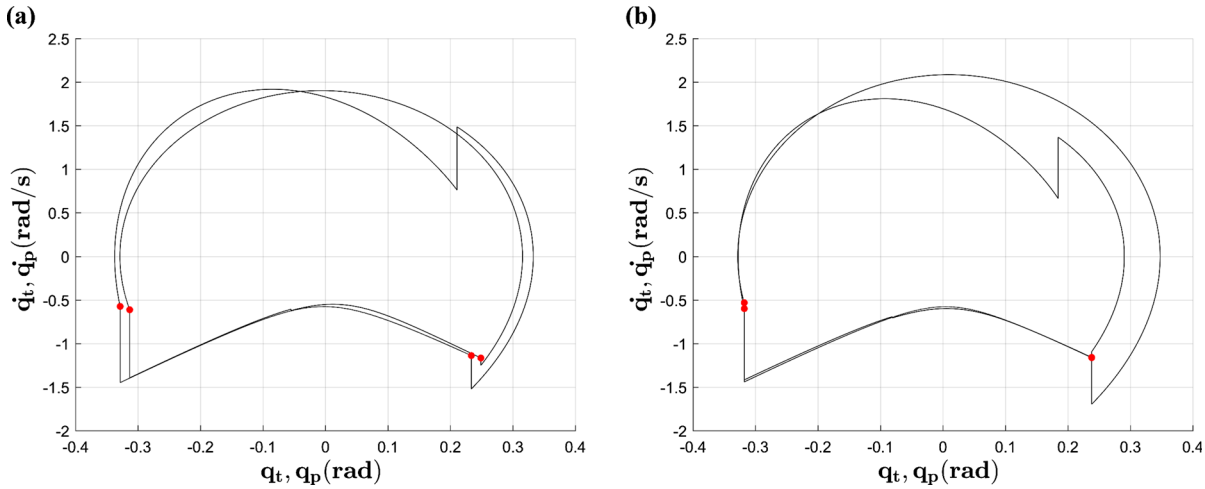

Fig. 16 Limit cycles of the thigh of the kneed leg and the knee-less leg for the model with symmetrical inertial parameters (**a**) and the model with symmetrical half inter-leg angles at the beginning of steps (**b**)

this issue, we can assume that the knee-less leg is made of two point masses with adjustable positions while the mass values are equal to the mass of the thigh and the shank of the kneed leg indicated by m_{tp} and m_{sp}. The positions of these masses can be calculated for different values of center of mass and the mass moment of inertia of the knee-less leg. We also assume that the position of the point mass with the higher mass value, x_{tp}, is above the point mass with the value equal to the mass of the shank x_{sp}. The relation between the positions of these masses for a required center of mass can be calculated as follows:

$$m_p a_p = m_{\text{tp}} x_{\text{tp}} + m_{\text{sp}} x_{\text{sp}}, \tag{32}$$

$$x_{\text{sp}} = \frac{m_p a_p - m_{\text{tp}} x_t}{m_{\text{sp}}} \tag{33}$$

The mass moment of inertia of the knee-less leg about the center of mass is obtained as follows:

$$J_p = m_{\text{tp}} \left(x_{\text{tp}} - a_p\right)^2 + m_{\text{sp}} \left(a_p - x_{\text{sp}}\right)^2 \tag{34}$$

By using Eq. (33), we can rewrite Eq. (34) in the form of Eq. (35):

$$A x_{\text{tp}}^2 + B x_{\text{tp}} + C = 0, \tag{35}$$

where A, B and C are:

$$A = \frac{m_{\text{tp}}^2}{m_{sp}} + m_{\text{tp}}, \tag{36}$$

$$B = 2 m_{\text{tp}} \left(ap - \frac{a_p m_p}{m_{\text{sp}}}\right) - 2 a_p m_{\text{tp}}, \tag{37}$$

$$C = a_p^2 m_{\text{tp}} - J_p + m_{\text{sp}} \left(a_p - \frac{a_p m_p}{m_{\text{sp}}}\right)^2 \tag{38}$$

Two sets of values for x_{tp} and x_{sp} are found by solving Eq. (35) where only one set satisfies the assumption $x_{\text{tp}} > x_{\text{sp}}$. There is a maximum possible value for the mass moment of inertia which occurs when the point masses are located at the two ends of the knee-less leg.

The mass moments of inertia that result in a symmetrical half inter-leg angle for different slope angles are displayed in Fig. 18, and the required location of the point masses for these values is displayed in Figs. 19 and 20 for x_{sp} and x_{tp}, respectively.

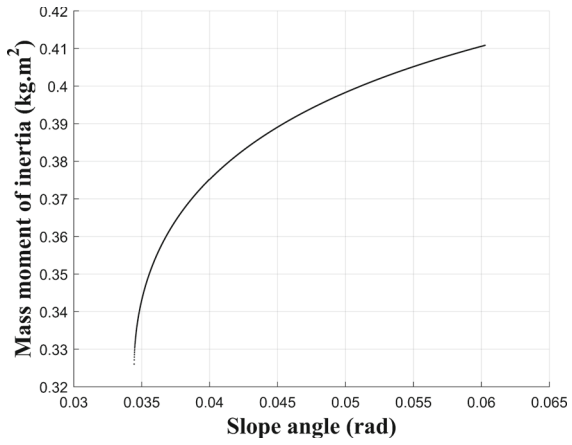

Fig. 18 Mass moments of inertia that result in a symmetrical half inter-leg angle for different slope angles for $c = 0.18 \frac{\text{Nms}}{\text{rad}}$ and symmetrical mass and COM values

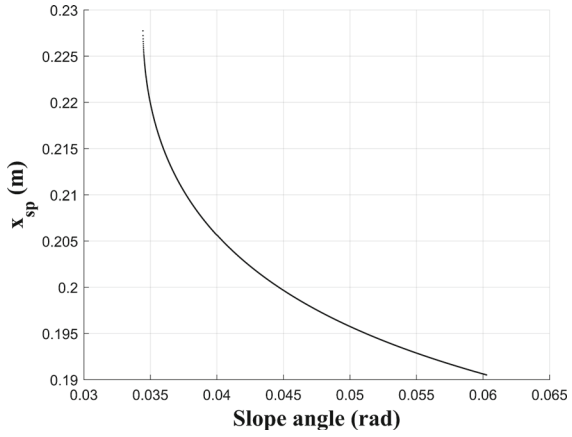

Fig. 19 Position of the shank point mass in the knee-less leg required to produce the mass moment of inertia displayed in Fig. 18 for different slope angles

3.3 Comparison of the asymmetric walker with a symmetric kneed walker

We have shown the method for finding a gait with symmetrical step lengths with a knee-less leg that consists of two point masses. The gait patterns with this characteristic, however, may provide additional benefits. The healthy leg of patients with unilateral lower-limb amputation will show deviations from its natural motion to compensate for the lost limb [38]. Consequently, we compare the motion of the asymmetric walker with a symmetric passive walker with two knees. The legs of this symmetric walker will possess inertial parameters similar to those of the

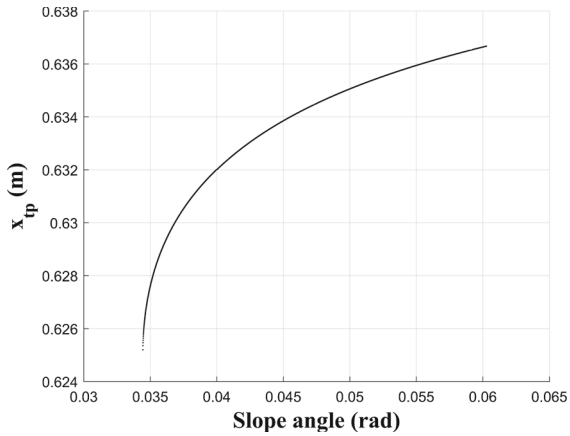

Fig. 20 Position of the thigh point mass in the knee-less leg required to produce the mass moment of inertia displayed in Fig. 18 for different slope angles

kneed leg of the asymmetric walker. Interestingly, the fixed point for the asymmetric walker lies in the basin of attraction of a steady 1-periodic gait for the symmetric walker on the same slope angle with similar damping coefficients in knees. To study the differences between these two models, we first compare the limit cycles of the shank and the thigh of the symmetric walker, with those of the kneed leg in the three-link walker with symmetrical inertial values. As expected, the limit cycles shown in Fig. 21 differ for these two models, meaning that by replacing one leg of the symmetric walker with a knee-less one with similar inertial parameters, the natural asymmetrical dynamics of the new system forces the remaining kneed leg to travel on a new trajectory.

By comparing the limit cycles of the symmetric walker with the three-link walker with symmetrical step lengths in Fig. 22, we observe that the limit cycles of the shank and the thigh of one leg of the symmetric walker are almost identical to those of the kneed leg of the asymmetric walker. This means that by replacing a leg in the symmetric walker with a knee-less leg of the three-link walker with symmetrical step lengths, the trajectory and the dynamic behavior of the remaining kneed leg will be unaltered.

4 Conclusion

In this paper, we found stable 2-periodic gait patterns for an asymmetric three-link passive walker with humanlike inertial parameters that consist of one kneed leg and a knee-less leg and studied the effects of changing the inertial parameters of the knee-less leg. Furthermore, we showed that by reducing the mass moment of inertia of the knee-less leg, it is possible to obtain a gait with symmetrical half inter-leg angles at the beginning of steps which results in a more symmetrical looking gait where the steps taken by the kneed and the knee-less leg will have equal length. We proposed a two point-mass system with adjustable positions for the knee-less leg that can make the gaits with symmetrical step lengths possible over different slope angles. Moreover, a comparison

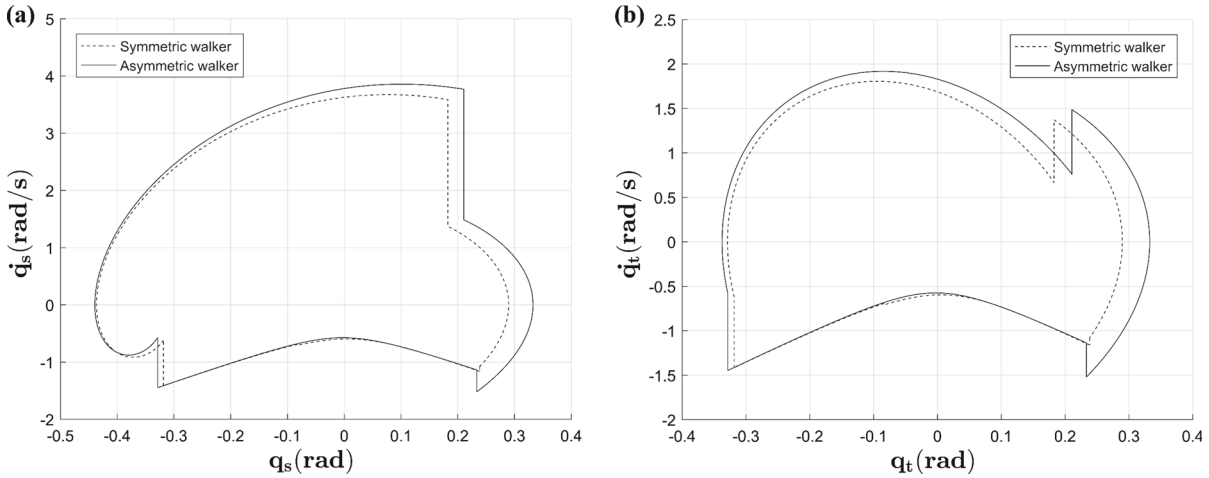

Fig. 21 Comparison of the limit cycles of the shank (**a**) and the thigh (**b**) of the kneed legs between the three-link asymmetric walker with symmetrical inertial parameters and the symmetric walker with similar inertial parameters

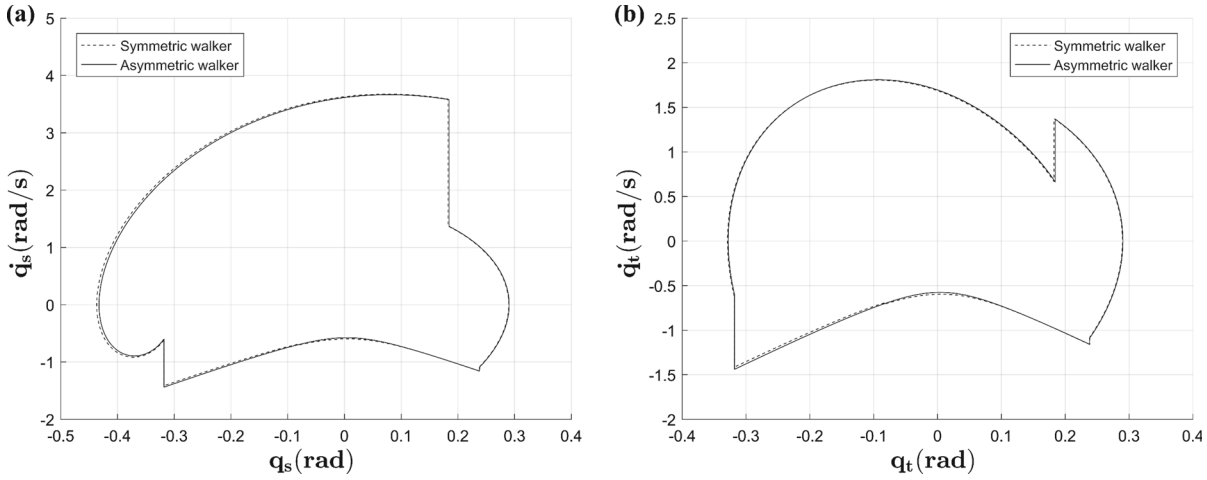

Fig. 22 Comparison of the limit cycles of the shank (**a**) and the thigh (**b**) of the kneed legs between the three-link asymmetric walker with symmetrical half inter-leg angles and the symmetric walker with inertial parameters equal to the kneed leg of the asymmetric walker

between the asymmetric walker and a symmetric walker with two kneed legs is made. This comparison shows that by replacing one leg of the symmetric walker with the knee-less leg of the three-link walker with symmetrical step lengths, the dynamic behavior of the remaining kneed leg will not be altered and it will travel on the path it did before. A similar approach can be adapted in the development of assistive devices to reduce the asymmetric characteristics of the gaits. Furthermore, the deviations from normal gaits, that are present in the healthy leg of unilateral lower-limb amputees, may be reduced by performing similar analyses for the physical parameters of prosthetic limbs.

Author's contribution All authors contributed to the study and the discussion of the presented results. BB conceived the original idea and developed the theory. The numerical simulations were performed by MJM. The first draft of the manuscript was written by MJM, and BB approved and finalized the manuscript to be published.

Funding The authors declare that no funds, grants, or other support were received during the preparation of this manuscript.

Data availability Data sharing is not applicable to this article as no datasets were generated or analyzed during the current study.

Declarations

Conflict of interest The authors have no relevant financial or non-financial interests to disclose.

References

1. Sakagami, Y., Watanabe, R., Aoyama, C., Matsunaga, S., Higaki, N. and Fujimura, K.: The intelligent ASIMO: system overview and integration. In IEEE/RSJ International Conference on Intelligent Robots and Systems (Vol. 3, pp. 2478–2483) (2002). IEEE. https://doi.org/10.1109/IRDS.2002.1041641
2. McGeer, T.: Passive dynamic walking. Int. J. Robot. Res. **9**(2), 62–82 (1990). https://doi.org/10.1177/027836499000900206
3. McGeer, T.: Passive walking with knees. In: IEEE International Conference on Robotics and Automation, Proceedings. IEEE (1990) https://doi.org/10.1109/ROBOT.1990.126245
4. Garcia, M., Chatterjee, A., Ruina, A., Coleman, M.: The simplest walking model: stability, complexity, and scaling. ASME J. Biomech. Eng. **120**, 281–288 (1998). https://doi.org/10.1115/1.2798313
5. Goswami, A., Thuilot, B., Espiau, B.: Compass-like biped robot part I: stability and bifurcation of passive gaits. INRIA (1996)
6. Das, S.L., Chatterjee, A.: An alternative stability analysis technique for the simplest walker. Nonlinear Dyn. **28**(3), 273–284 (2002). https://doi.org/10.1023/A:1015685325992
7. Schwab, A.L. and Wisse, M.: Basin of attraction of the simplest walking model. In International Design Engineering Technical Conferences and Computers and Information in Engineering Conference (Vol. 80272, pp. 531–539). American Society of Mechanical Engineers. (2001) https://doi.org/10.1115/DETC2001/VIB-21363

8. Montazeri Moghadam, S., Sadeghi Talarposhti, M., Niaty, A., Towhidkhah, F., Jafari, S.: The simple chaotic model of passive dynamic walking. Nonlinear Dyn. **93**(3), 1183–1199 (2018). https://doi.org/10.1007/s11071-018-4252-8
9. Wisse, M., Hobbelen, D.G., Rotteveel, R.J., Anderson, S.O. and Zeglin, G.J.: Ankle springs instead of arc-shaped feet for passive dynamic walkers. In 2006 6th IEEE-RAS International Conference on Humanoid Robots (pp. 110–116) (2006). IEEE. https://doi.org/10.1109/ICHR.2006.321371
10. Zang, X., Liu, X., Liu, Y., Iqbal, S., Zhao, J.: Influence of the swing ankle angle on walking stability for a passive dynamic walking robot with flat feet. Adv. Mech. Eng. **8**(3), 1687814016642018 (2016). https://doi.org/10.1177/1687814016642018
11. Liu, X., Zang, X., Zhu, Y., Liu, Y., Zhao, J.: System overview and walking dynamics of a passive dynamic walking robot with flat feet. Adv. Mech. Eng. **7**(12), 1687814015620967 (2015). https://doi.org/10.1177/1687814015620967
12. Wang, Q., Huang, Y., Wang, L.: Passive dynamic walking with flat feet and ankle compliance. Robotica **28**(3), 413–425 (2010). https://doi.org/10.1017/S0263574709005736
13. Borzova, E., Hurmuzlu, Y.: Passively walking five-link robot. Automatica **40**(4), 621–629 (2004). https://doi.org/10.1016/j.automatica.2003.10.015
14. Wisse, M., Schwab, A.L., Van Der Helm, F.C.T.: Passive dynamic walking model with upper body. Robotica **22**, 681–688 (2004). https://doi.org/10.1017/S0263574704000475
15. Adolfsson, J., Dankowicz, H., Nordmark, A.: 3D passive walkers: finding periodic gaits in the presence of discontinuities. Nonlinear Dyn. **24**(2), 205–229 (2001). https://doi.org/10.1023/A:1008300821973
16. Wisse, M. and Frankenhuyzen, J.V.: Design and construction of mike; a 2-d autonomous biped based on passive dynamic walking. In Adaptive motion of animals and machines (pp. 143–154). Springer, Tokyo. (2006) https://doi.org/10.1007/4-431-31381-8_13
17. Collins, S.H., Wisse, M., Ruina, A.: A three-dimensional passive-dynamic walking robot with two legs and knees. Int. J. Robot. Res. **20**(7), 607–615 (2001). https://doi.org/10.1177/02783640122067561
18. Wang, K., Tobajas, P.T., Liu, J., Geng, T., Qian, Z., Ren, L.: Towards a 3D passive dynamic walker to study ankle and toe functions during walking motion. Robot. Auton. Syst. **115**, 49–60 (2019). https://doi.org/10.1016/j.robot.2019.02.010
19. Sabaapour, M.R., Hairi Yazdi, M.R., Beigzadeh, B.: Passive turning motion of 3D rimless wheel: novel periodic gaits for bipedal curved walking. Adv. Robot. **29**(5), 375–384 (2015). https://doi.org/10.1080/01691864.2014.1001788
20. Sabaapour, M.R., Hairi Yazdi, M.R., Beigzadeh, B.: Passive dynamic turning in 3D biped locomotion: an extension to passive dynamic walking. Adv. Robot. **30**(3), 218–231 (2016). https://doi.org/10.1080/01691864.2015.1107500
21. Beigzadeh, B., Sabaapour, M.R., Yazdi, M.R.H., Raahemifar, K.: From a 3d passive biped walker to a 3d passivity-based controlled robot. Int. J. Humanoid Rob. **15**(04), 1850009 (2018). https://doi.org/10.1142/S0219843618500093
22. Kobayashi, T., Aoyama, T., Hasegawa, Y., Sekiyama, K., Fukuda, T.: Adaptive speed controller using swing leg motion for 3-D limit-cycle-based bipedal gait. Nonlinear Dyn. **84**(4), 2285–2304 (2016). https://doi.org/10.1007/s11071-016-2645-0
23. Gritli, H., Belghith, S., Khraief, N.: OGY-based control of chaos in semi-passive dynamic walking of a torso-driven biped robot. Nonlinear Dyn. **79**(2), 1363–1384 (2015). https://doi.org/10.1007/s11071-014-1747-9
24. Gritli, H., Belghith, S.: Bifurcations and chaos in the semi-passive bipedal dynamic walking model under a modified OGY-based control approach. Nonlinear Dyn. **83**(4), 1955–1973 (2016). https://doi.org/10.1007/s11071-015-2458-6
25. Znegui, W., Gritli, H., Belghith, S.: Stabilization of the passive walking dynamics of the compass-gait biped robot by developing the analytical expression of the controlled Poincaré map. Nonlinear Dyn. **101**(2), 1061–1091 (2020). https://doi.org/10.1007/s11071-020-05851-9
26. Fenili, A., Balthazar, J.M.: The rigid-flexible nonlinear robotic manipulator: modeling and control. Commun. Nonlinear Sci. Numer. Simul. **16**(5), 2332–2341 (2011). https://doi.org/10.1016/j.cnsns.2010.04.057
27. Beigzadeh, B., Meghdari, A., Sohrabpour, S.: Passive dynamic object manipulation: preliminary definition and examples. Acta Autom. Sin. **36**(12), 1711–1719 (2010). https://doi.org/10.1016/S1874-1029(09)60067-7
28. Beigzadeh, B., Meghdari, A., and Sohrabpour, S.: Passive dynamic object manipulation: A framework for passive walking systems. Proceedings of the Institution of Mechanical Engineers, Part K: Journal of Multi-body Dynamics, 227(2), pp. 185–198. (2013) https://doi.org/10.1177/1464419313478525
29. Sushko, J., Honeycutt, C., and Reed, K.B.: Prosthesis design based on an asymmetric passive dynamic walker. In 2012 4th IEEE RAS & EMBS International Conference on Biomedical Robotics and Biomechatronics (BioRob) (pp. 1116–1121) (2012). IEEE. https://doi.org/10.1109/BioRob.2012.6290293
30. Wang, D., Lee, K.M., Ji, J.: A passive gait-based weight-support lower extremity exoskeleton with compliant joints. IEEE Trans. Rob. **32**(4), 933–942 (2016). https://doi.org/10.1109/TRO.2016.2572692
31. Apte, S., Plooij, M., Vallery, H.: Simulation of human gait with body weight support: benchmarking models and unloading strategies. J. Neuroeng. Rehabil. **17**(1), 1–16 (2020). https://doi.org/10.1186/s12984-020-00697-z
32. Honeycutt, C., Sushko, J., and Reed, K.B.: Asymmetric passive dynamic walker. In 2011 IEEE International Conference on Rehabilitation Robotics (pp. 1–6) (2011). IEEE. https://doi.org/10.1109/icorr.2011.5975465
33. Beigzadeh, B., Razavi, S.A.: Dynamic walking analysis of an underactuated biped robot with asymmetric structure. Int. J. Humanoid Rob. **18**(04), 2150014 (2021). https://doi.org/10.1142/s0219843621500146
34. Little, V.L., Perry, L.A., Mercado, M.W., Kautz, S.A., Patten, C.: Gait asymmetry pattern following stroke determines acute response to locomotor task. Gait Posture **77**,

300–307 (2020). https://doi.org/10.1016/j.gaitpost.2020.02.016
35. Barnett, C., Vanicek, N., Polman, R., Hancock, A., Brown, B., Smith, L., Chetter, I.: Kinematic gait adaptations in unilateral transtibial amputees during rehabilitation. Prosthet. Orthot. Int. **33**(2), 135–147 (2009). https://doi.org/10.1080/03093640902751762
36. Dumas, R. and Wojtusch, J.: Estimation of the Body Segment Inertial Parameters for the Rigid Body Biomechanical Models Used in Motion Analysis. In: Müller B., Wolf S. (eds.) Handbook of Human Motion. (2018)
37. Westervelt, E.R., Grizzle, J.W., Chevallereau, C., Choi, J.H., Morris, B.: Feedback Control of Dynamic Bipedal Robot Locomotion. CRC Press, Boca Raton (2018)
38. Highsmith, M.J., Andrews, C.R., Millman, C., Fuller, A., Kahle, J.T., Klenow, T.D., Lewis, K.L., Bradley, R.C., Orriola, J.J.: Gait training interventions for lower extremity amputees: a systematic literature review. Technol. Innov. **18**(2–3), 99–113 (2016). https://doi.org/10.21300/18.2-3.2016.99